Shape-Selective Enantioselective Hydrogenation on Pt Nanoparticles

Erik Schmidt, Angelo Vargas, Tamas Mallat, and Alfons Baiker*

Department of Chemistry and Applied Biosciences, ETH Zürich, Hönggerberg, HCI, CH-8093, Zürich, Switzerland

Received May 28, 2009; E-mail: baiker@chem.ethz.ch

Abstract: The structure sensitivity of enantioselective hydrogenations on chirally modified metals was investigated using Pt nanoparticles of different shapes. All three samples had an average particle size of 10 nm, but the fraction of dominantly cubic, cubooctahedral, and octahedral particles varied with decreasing {100} and increasing {111} faces in the same order. In the absence of chiral modifier the hydrogenation of ethyl pyruvate was independent of the shape of the Pt nanoparticles; variation of the specific reaction rates did not exceed the experimental error on all self-prepared catalysts and on a commercial Pt/Al$_2$O$_3$ used as reference. Addition of cinchonidine or quinine induced a significant rate enhancement by a factor of 4−15, and the rate was always higher with quinine. Also, 72−92% ees were achieved, and the reaction was shape selective: both the rate and the ee increased with increasing Pt{111}/Pt{100} ratio. A similar correlation in the hydrogenation of ketopantolactone confirmed that decarbonylation or aldol-type side reactions of ethyl pyruvate were not the reason for structure sensitivity. A combined catalytic and theoretical study revealed that the probable origin of the particle shape dependency of enantioselective hydrogenation is the adsorption behavior of the cinchona alkaloid. DFT studies of cinchonidine interacting with Pt(100) and Pt(111) terraces indicated a remarkably stronger interaction on the former crystallographic face by ca. 155 kJ/mol. The higher adsorption strength on Pt(100) was corroborated experimentally by the faster hydrogenation of the homoaromatic ring of the alkaloid, which fragment interacts the strongest with Pt during its adsorption. Thus, an ideal catalyst for the hydrogenation of activated ketones contains dominantly Pt{111} terraces, which crystallographic face is more active and affords higher enantioselectivity, combined with the higher stability of the modifier.

1. Introduction

There has been an impressive development in the past years in heterogeneous enantioselective catalysis. The simple strategy of using a conventional (supported) metal catalyst in the presence of a chiral compound that provides the suitable stereochemical control led to high enantioselectivities in various reactions.[1−6] Theoretical calculations of the adsorption of the chiral modifier on model metal surfaces represent the first step toward rationalization of the experimental observations.[7−14] The surface science studies on chirally modified metals helped to gain a closer insight into the interaction of the substrate and the chiral modifier with the metal surface and led to novel concepts for the origin of enantioselection.[15−23]

Despite this progress, there is still a significant gap between the catalytic-synthetic approach focusing on the development of highly enantioselective catalyst systems and the theoretical and surface science routes that apply idealized conditions to allow a better understanding of the phenomena. An example is

(1) Mallat, T.; Orglmeister, E.; Baiker, A. *Chem. Rev.* **2007**, *107*, 4863−4890.
(2) Bartók, M. *Curr. Org. Chem.* **2006**, *10*, 1533−1567.
(3) Blaser, H. U.; Studer, M. *Acc. Chem. Res.* **2007**, *40*, 1348−1356.
(4) Murzin, D. Y.; Maki-Arvela, P.; Toukoniitty, E.; Salmi, T. *Catal. Rev.-Sci. Eng.* **2005**, *47*, 175−256.
(5) Tungler, A.; Sipos, E.; Hada, V. *Curr. Org. Chem.* **2006**, *10*, 1569−1583.
(6) Tai, A.; Sugimura, T. In *Chiral Catalyst Immobilization and Recycling*; DeVos, D. E., Vankelecom, I. F. J., Jacobs, P. A., Eds.; Wiley-VCH: Weinheim, 2000; pp 173−209.
(7) Schwalm, O.; Weber, J.; Margitfalvi, J.; Baiker, A. *J. Mol. Struct.* **1993**, *297*, 285−293.
(8) Simons, K. E.; Meheux, P. A.; Griffiths, S. P.; Sutherland, I. M.; Johnston, P.; Wells, P. B.; Carley, A. F.; Rajumon, M. K.; Roberts, M. W.; Ibbotson, A. *Recl. Trav. Chim. Pays-Bas* **1994**, *113*, 465−474.
(9) Bürgi, T.; Baiker, A. *Acc. Chem. Res.* **2004**, *37*, 909−917.
(10) Avery, K. A.; Mann, R.; Norton, M.; Willock, D. J. *Top. Catal.* **2003**, *25*, 89−102.
(11) Calvo, S. R.; LeBlanc, R. J.; Williams, C. T.; Balbuena, P. B. *Surf. Sci.* **2004**, *563*, 57−73.
(12) Taskinen, A.; Nieminen, V.; Hotokka, M.; Murzin, D. Y. *J. Phys. Chem. C* **2007**, *111*, 5128−5140.
(13) Vargas, A.; Santarossa, G.; Iannuzzi, M.; Baiker, A. *J. Phys. Chem. C* **2008**, *112*, 10200−10208.
(14) Vargas, A.; Bürgi, T.; Baiker, A. *J. Catal.* **2004**, *226*, 69−82.
(15) Ferri, D.; Bürgi, T. *J. Am. Chem. Soc.* **2001**, *123*, 12074−12084.
(16) Zaera, F. *J. Phys. Chem. C* **2008**, *112*, 16196−16203.
(17) Laliberte, M. A.; Lavoie, S.; Hammer, B.; Mahieu, G.; McBreen, P. H. *J. Am. Chem. Soc.* **2008**, *130*, 5386−5387.
(18) Schmidt, E.; Ferri, D.; Vargas, A.; Baiker, A. *J. Phys. Chem. C* **2008**, *112*, 3866−3874.
(19) Baddeley, C. J. *Top. Catal.* **2003**, *25*, 17−28.
(20) LeBlanc, R. J.; Chu, W.; Williams, C. T. *J. Mol. Catal. A: Chem.* **2004**, *212*, 277−289.
(21) Bakos, I.; Szabó, S.; Bartók, M.; Kálmán, E. *J. Electroanal. Chem.* **2002**, *532*, 113−119.
(22) Bonello, J. M.; Lindsay, R.; Santra, A. K.; Lambert, R. M. *J. Phys. Chem. B* **2002**, *106*, 2672−2679.
(23) Schmidt, E.; Ferri, D.; Baiker, A. *Langmuir* **2007**, *23*, 8087−8093.

the early observation of a remarkable selectivity enhancement by a reductive treatment of supported Pt prior to the hydrogenation of α-ketoesters.[24] It was shown later that treatment of Pt/Al₂O₃ in flowing hydrogen at elevated temperature doubled the enantioselectivity, as compared to the treatment in air under otherwise identical conditions.[25] The shift in enantioselectivity was reversible by changing the gas atmosphere, and redispersion of the Pt particles was evidenced by HRTEM. The effect of heat treatment was attributed to adsorbate, i.e., hydrogen and oxygen, induced restructuring,[26] but no evidence for the change in the surface morphology of Pt has been found. Another efficient catalyst pretreatment method is ultrasonication,[27,28] and its positive effect on the enantioselection is probably also linked to changes in the morphology of the metal particles. In the hydrogenation of 3,5-di(trifluoromethyl)acetophenone, the enantioselectivity more than tripled after stirring the catalyst slurry under nitrogen in the presence of cinchonidine or quinoline prior to the reaction.[29] Catalyst restructuring due to reactive adsorption of the heteroaromatic compounds was confirmed by electron microscopy, but no correlation between surface morphology and enantioselectivity could be derived.

The structure sensitivity[30] of heterogeneous catalytic reactions is commonly investigated by varying the size of the metal particles in the range 1−20 nm.[31−34] The biggest changes of proportions between the high- and low-coordinated surface sites occur between 1 and 5 nm.[35] There are numerous reports on the structure sensitivity of hydrogenations on chirally modified Pt-group metals and Ni,[1,4,36−38] but the results are contradictory. For example, it was earlier described that in the hydrogenation of pyruvate esters on cinchonidine-(CD)-modified Pt/Al₂O₃ the rate and enantioselectivity increased with increasing Pt particle size up to 3−4 nm.[39] A feasible explanation for the poor enantioselectivity characteristic of metal particles below 2 nm is a geometric effect:[40,41] the small particles cannot accommodate the bulky modifier−substrate complex that occupies 20−25 surface atoms,[9] and the nonmodified reaction leads to a racemic product. But this concept is in contrast to the excellent

enantioselectivity (97.6% ee) achieved in the same reaction using tiny Pt nanoparticles with a narrow particle size distribution (1.4 ± 0.2 nm).[42]

Here we report another approach to reduce the gap between surface science and practical catalysis. We synthesized Pt nanoparticles of different shapes but very similar size and tested them in the enantioselective hydrogenation of an α-ketoester and an α-ketolactone. The efficiency of this approach is well documented in the study of the influence of surface morphology of metal nanoparticles on the reaction rate and chemoselectivity.[43] The reactions include hydrogenation and dehydrogenation,[44−46] oxidation and electrooxidation,[46−51] isomerization,[52] and oxygen reduction.[53] Since our focus is on the role of surface morphology in enantioselection, we choose a method that provides relatively big particles of ∼10 nm with a narrow particle size distribution.[54] Thus, the effect of particle size can be eliminated and the observed differences in enantioselectivity can be unambiguously correlated with the surface morphology of Pt.

2. Experimental Section

2.1. Materials. Pt colloids with a controlled shape have been synthesized by reduction of an aqueous solution of K₂PtCl₄ (Aldrich, 99.9+%) with H₂ (PanGas, 5.0), according to a method described in the literature.[54] Different Pt particle shape distributions were achieved by varying the concentration of the colloid stabilizer poly(acrylic acid) (PAA, Aldrich, M_W = 2100). The preparation of the samples Pt-1, Pt-2, and Pt-3 was conducted at Pt:PAA molar ratios of 1:1, 1:3, and 1:5, respectively.

For the preparation of Pt-1/SiO₂, Pt-2/SiO₂, and Pt-3/SiO₂, a suspension of SiO₂ (Degussa, Aerosil 200) in water was prepared by sonification and added to the Pt colloidal solution. After stirring for 1 h the colloids were deposited onto silica by dropwise acidification until pH = 2 (0.1 M HCl). The samples containing 5 wt % Pt were filtered off, washed with water (10 times) to remove excess PAA, and dried overnight at 60 °C and 10 mbar. Silica was chosen as the support because of the superior resolution of the TEM pictures, compared to Al₂O₃. One colloidal solution (sample Pt-1) was divided into two fractions and deposited onto SiO₂ and Al₂O₃ (Degussa, Aluminum oxide C) to allow a direct comparison to the commercial catalyst Pt/Al₂O₃ (Engelhard 4759), which was chosen

(24) Orito, Y.; Imai, S.; Niwa, S. *J. Chem. Soc. Jpn.* **1979**, 1118−1120.
(25) Mallat, T.; Frauchiger, S.; Kooyman, P. J.; Schürch, M.; Baiker, A. *Catal. Lett.* **1999**, *63*, 121−126.
(26) Somorjai, G. A.; Park, J. Y. *Angew. Chem., Int. Ed.* **2008**, *47*, 9212−9228.
(27) Török, B.; Felföldi, K.; Szakonyi, G.; Balázsik, K.; Bartók, M. *Catal. Lett.* **1998**, *52*, 81−84.
(28) Török, B.; Balázsik, K.; Felföldi, K.; Bartók, M. *Ultrason. Sonochem.* **2001**, *8*, 191−200.
(29) Hess, R.; Krumeich, F.; Mallat, T.; Baiker, A. *Catal. Lett.* **2004**, *92*, 141−148.
(30) Boudart, M. *Adv. Catal.* **1969**, *20*, 153−166.
(31) Che, M.; Bennett, C. O. *Adv. Catal.* **1989**, *36*, 55−172.
(32) Coq, B.; Figueras, F. *Coord. Chem. Rev.* **1998**, *180*, 1753−1783.
(33) Guczi, L.; Petö, G.; Beck, A.; Pászti, Z. *Top. Catal.* **2004**, *29*, 129−138.
(34) VanSanten, R. A. *Acc. Chem. Res.* **2009**, *42*, 57−66.
(35) VanHardeveld, R.; Hartog, F. *Surf. Sci.* **1969**, *15*, 189−230.
(36) Bönnemann, H.; Braun, G. A. *Angew. Chem., Int. Ed. Engl.* **1996**, *35*, 1992−1995.
(37) Zuo, X.; Liu, H.; Guo, D.; Yang, X. *Tetrahedron* **1999**, *55*, 7787−7804.
(38) Nitta, Y.; Kubota, T.; Okamoto, Y. *Bull. Chem. Soc. Jpn.* **2000**, *73*, 2635−2641.
(39) Wehrli, J. T.; Baiker, A.; Monti, M.; Blaser, H. U. *J. Mol. Catal.* **1990**, *61*, 207−226.
(40) Jackson, S. D.; Keegan, M. B. T.; McLellan, G. D.; Meheux, P. A.; Moyes, R. B.; Webb, G.; Wells, P. B.; Whyman, R.; Willis, J. In *Studies in Surface Science and Catalysis*; Poncelet, G., Jacobs, P. A., Grange, G., Delmon, B., Eds.; Elsevier: Amsterdam, 1991; p 135.
(41) Hoxha, F.; Vegten, N. V.; Urakawa, A.; Krumeich, F.; Mallat, T.; Baiker, A. *J. Catal.* **2009**, *261*, 224−231.
(42) Zuo, X.; Liu, H.; Liu, M. *Tetrahedron Lett.* **1998**, *39*, 1941−1944.
(43) Burda, C.; Chen, X. B.; Narayanan, R.; El-Sayed, M. A. *Chem. Rev.* **2005**, *105*, 1025−1102.
(44) Lee, H.; Habas, S. E.; Kweskin, S.; Butcher, D.; Somorjai, G. A.; Yang, P. *Angew. Chem., Int. Ed.* **2006**, *45*, 7824−7828.
(45) Somorjai, G. A.; Park, J. Y. *J. Chem. Phys.* **2008**, *128*, 182504−11824504−9.
(46) Serrano-Ruiz, J. C.; López-Cudero, A.; Solla-Gullón, J.; Sepúlveda-Escribano, A.; Aldaz, A.; Rodríguez-Reinoso, F. *J. Catal.* **2008**, *253*, 159−166.
(47) Vidal-Iglesias, F. J.; Solla-Gullon, J.; Rodriguez, P.; Herrero, E.; Montiel, V.; Feliu, J. M.; Aldaz, A. *Electrochem. Commun.* **2004**, *6*, 1080−1084.
(48) Xu, R.; Wang, D. S.; Zhang, J. T.; Li, Y. D. *Chem.—Asian J.* **2006**, *1*, 888−893.
(49) Park, K. H.; Jang, K.; Kim, H. J.; Son, S. U. *Angew. Chem., Int. Ed.* **2007**, *46*, 1152−1155.
(50) Subhramannia, M.; Pillai, V. K. *J. Mater. Chem.* **2008**, *18*, 5858−5870.
(51) Solla-Gullon, J.; Vidal-Iglesias, F. J.; Lopez-Cudero, A.; Garnier, E.; Feliu, J. M.; Aldaza, A. *Phys. Chem. Chem. Phys.* **2008**, *10*, 3689−3698.
(52) Lee, I.; Delbecq, F.; Morales, R.; Albiter, M. A.; Zaera, F. *Nat. Mater.* **2009**, *8*, 132−138.
(53) Wang, C.; Daimon, H.; Onodera, T.; Koda, T.; Sun, S. *Angew. Chem., Int. Ed.* **2008**, *47*, 3588−3591.
(54) Ahmadi, T. S.; Wang, Z. L.; Green, T. C.; Henglein, A.; El-Sayed, M. A. *Science* **1996**, *272*, 1924−1926.

as reference because it is the best known and mostly used catalyst in the enantioselective hydrogenation of ketones.

Before the catalytic experiments, ethyl pyruvate (Acros, 98%) was freshly distilled and toluene (Fluka, 99.7%) was dried over an activated molecular sieve. Ketopantolactone (Roche, 99%), acetic acid (Acros, 99.8%), cinchonidine (CD, Fluka, >98% alkaloid), and quinine (QN, Fluka, >99% alkaloid) were used as received.

2.2. Methods. For TEM investigations, the material was deposited onto a holey carbon foil supported on a copper grid. The measurements were performed with a CM30ST microscope (FEI; LaB$_6$ cathode, operated at 300 kV, point resolution ~2 Å). Scanning transmission electron microscopic (STEM) images were recorded with a high-angle annular dark field (HAADF) detector at a Tecnai F30 microscope (FEI; field emission gun, operated at 300 kV, point resolution ~2 Å). HAADF-STEM images reveal the metal particles with bright contrast (Z contrast). Energy dispersive X-ray spectroscopy (EDS) was used to distinguish between the metal particles and the support. An EDAX system attached to the Tecnai F30 microscope was used for the EDS experiments.

The Pt content of the catalysts was determined with atomic absorption spectroscopy (AAS) on a Varian SpectrAA 220 FS spectrometer equipped with an air/C$_2$H$_2$ burner and a D$_2$-lamp for background correction. The samples were dissolved in a HF/aqua regia mixture overnight.

X-ray photoelectron spectroscopic (XPS) analysis of the Pt nanoparticles deposited onto SiO$_2$ was performed on a Leybold Heraeus LHS11 MCD instrument using Mg K$_\alpha$ (1253.6 eV) radiation. The sample was pressed into a sample holder, evacuated in a load lock to 10^{-6} mbar, and transferred to the analysis chamber (typical pressure <10^{-9} mbar). The peaks were energy-shifted to the binding energy of Si 2p for SiO$_2$ (103.4 eV) to correct for the charging of the material. The surface composition of the catalysts was determined from the peak areas of Pt 4f, Si 2p, O 1s, Cl 2s, and C 1s, which were computed after subtraction of the Shirley-type background by empirically derived cross section factors.

The presence of the colloid stabilizer PAA on the Pt surface was confirmed by CO adsorption followed by DRIFTS on a Bruker Equinox 55 spectrometer, equipped with a liquid-nitrogen-cooled MCT detector. Samples were dried in flowing Ar (PanGas, 6.0; 20 mL/min) for 1 h before adsorption of CO (10% in He, 20 mL/min) for 90 min, followed by purging with Ar before the measurement.

2.3. Catalytic Hydrogenation. Hydrogenation of ethyl pyruvate was carried out in a magnetically stirred 50 mL glass reactor at 291 K under flowing hydrogen at ambient pressure.[55] The dried catalyst (21 ± 1 mg, 5 wt.% Pt) was stirred (750 rpm) in 9 mL of acetic acid for 5 min under flowing nitrogen followed by flowing hydrogen for 5 min. CD or QN as chiral modifier (3.4 μmol) and *n*-tetradecane as internal standard were injected in 1 mL of an acetic acid solution, followed by further stirring for 5 min under H$_2$. For experiments in the absence of modifier, 1 mL of neat acetic acid was used instead of the modifier solution. The reaction was started by injecting the substrate (0.33 mL, 4.0 mmol). Samples of the reaction mixture were filtered and diluted with ethyl acetate before GC analysis (Thermo Finnigan Trace 2000, CP-Chirasil-Dex CB capillary column, FID detector). The enantioselective reactions needed 3−10 h to reach full conversion of ethyl pyruvate. Both CD and QN afford the (*R*) enantiomer in excess. The TOFs were calculated from the linear part of the conversion−time plot (conversions below 80%) based on the fraction of surface Pt atoms (dispersion) as determined by TEM. The ee's were determined at full conversion. The slow reactions in the absence of a chiral modifier were stopped after 4 h, at 10−12% conversion.

Hydrogenation of ketopantolactone was performed in a 50 mL stainless steel reactor equipped with a glass-liner, PTFE cover and magnetic stirrer (750 rpm). The pressure was controlled by a constant-volume constant-pressure system (Büchi BPC 9901). According to a procedure described in the literature,[56] 5 mL of toluene containing 0.68 μmol of CD was mixed with 21 ± 1 mg of catalyst (5 wt.% Pt) before addition of 0.92 mmol of ketopantolactone. The reactions were carried out at 70 bar and 264 K for 30 min to ensure full conversion. The reaction rate was determined at ambient pressure (at 273 K in toluene using 10 mg of catalyst and 0.46 mmol of substrate) in the reactor used for the hydrogenation of ethyl pyruvate. Analysis and calculations were made analogous to those of ethyl pyruvate hydrogenation.

Hydrogenation of the aromatic ring system of CD was carried out under conditions identical to those used for hydrogenation of ethyl pyruvate but in the absence of the substrate. First, the reaction mixture was stirred under nitrogen for 5 min to allow the adsorption of the modifier on the catalyst surface. The reaction was started by switching the atmosphere to hydrogen. Samples of the reaction mixture were taken via syringe, the catalyst was filtered off, and the filtrate was diluted with acetic acid 5-fold before UV analysis on a Cary 400 spectrometer with a 10 mm path length quartz cuvette. The concentration of the modifier in solution used for estimating its conversion was determined with a calibration curve.

2.4. Computational Methods. All calculations have been performed with the CP2K program package suite of programs aimed at performing efficient electronic structure calculations and molecular dynamics at different levels of theory.[57] The electronic structure was modeled by means of Density Functional Theory (DFT), where the Kohn−Sham orbitals were expanded using the Gaussian and Plane Wave basis set formalism (GPW).[58,59] Within the GPW formalism, the wave function is described using Gaussian type orbitals (GTOs), with an auxiliary plane wave (PW) basis set expansion of the charge density. The GTOs have been expanded in terms of triple-ζ valence with double polarization (TZV2P) basis sets for H and second row elements and a triple-ζ valence (TZV) basis set with very confined functions (smallest exponent 0.1) for Pt. For the auxiliary PW basis set the energy cutoff has been set at 320 Ry. The interaction of the valence electrons with frozen atomic cores has been described *via* the use of norm-conserving, dual-space type pseudopotentials (PP).[60] For second row elements a PP that includes the first shell electrons has been used, while for Pt the PP included the 5s and 5p semicore electrons. The exchange and correlation term has been modeled using the Perdew−Burke−Ernzerhof (PBE) functional.[61]

The metal surfaces exposing the (111) and the (100) crystallographic planes have been modeled using a slab approach, where the semi-infinite bulk is approximated by a finite number of atomic layers, parallel to the desired crystallographic plane. The Pt(111) surface supercell was modeled by an orthorhombic cell constituted by four layers of (6 × 6) atoms per layer, piled along the *z* axis, for a total of 144 atoms (Figure 1a). The dimensions of the cell along the directions parallel to the surface are 16.82 and 14.56 Å. The Pt(100) surface supercell was modeled by an orthorhombic cell constituted by four layers of (4 × 4) atoms per layer, piled along the *z* axis, for a total of 128 atoms (Figure 1b). The resulting slab is separated from its periodic images in the direction perpendicular to the surface by interposing an adequate amount of empty space (more than 15 Å). The metal lattice constant was chosen according to the optimal theoretical value found for bulk Pt (3.965 Å).[62] The geometries have been optimized using the

(55) Huck, W.-R.; Mallat, T.; Baiker, A. *Adv. Synth. Catal.* **2003**, *345*, 255−260.

(56) Schürch, M.; Künzle, N.; Mallat, T.; Baiker, A. *J. Catal.* **1998**, *176*, 569−571.

(57) VandeVondele, J.; Krack, M.; Mohamed, F.; Parrinello, M.; Chassaing, T.; Hutter, J. *Comput. Phys. Commun.* **2005**, *167*, 103−128.

(58) VandeVondele, J.; Hutter, J. *J. Chem. Phys.* **2007**, *127*, 114105.

(59) VandeVondele, J.; Hutter, J. *J. Chem. Phys.* **2003**, *118*, 4365−4369.

(60) Goedecker, S.; Teter, M.; Hutter, J. *Phys. Rev. B* **1996**, *54*, 1703–1710.

(61) Perdew, J. P.; Burke, K.; Ernzerhof, M. *Phys. Rev. Lett.* **1996**, *77*, 3865–3868.

(62) Santarossa, G.; Vargas, A.; Iannuzzi, M.; Pignedoli, C. A.; Passerone, D.; Baiker, A. *J. Chem. Phys.* **2008**, *129*, 234703.
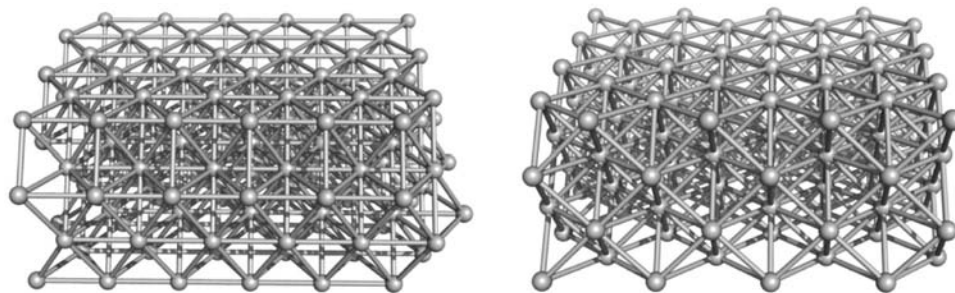
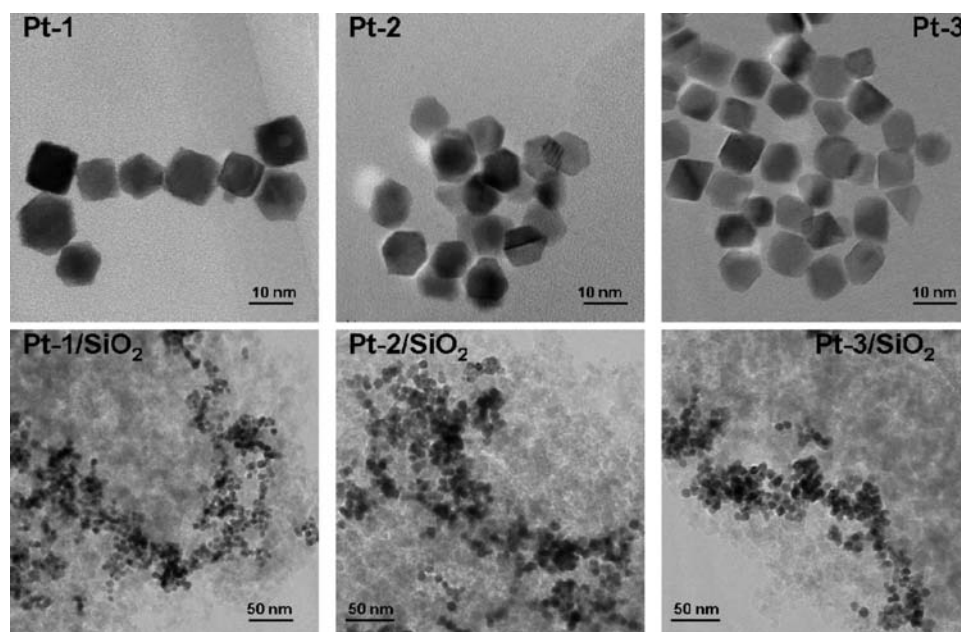**Figure 1.** Pt(111) and Pt(100) supercells used for adsorption studies.

Figure 2. Typical TEM pictures of PAA-stabilized platinum colloids Pt-1, Pt-2, and Pt-3 in aqueous solution (top series) and the corresponding silica-supported samples Pt-1/SiO$_2$, Pt-2/SiO$_2$, and Pt-3/SiO$_2$.

Broyden−Fletcher−Goldfarb−Shanno minimization algorithm (BFGS)[63−67] until the atomic displacements were lower than 3×10^{-3} bohr and the forces were lower than 4.5×10^{-4} Ha/bohr. For both cells the geometry optimizations were run by keeping the first layer of the slabs fixed, while all other degrees of freedom (top three metal layers and adsorbate molecule) were set free to optimize. The problem of the adsorption energy of CD on platinum has been addressed elsewhere,[13,68,69] while in this work we have focused on the differences between adsorption energies of CD on Pt(111) and Pt(100), which has been calculated as follows:

$$\text{En}_{\{\text{CD-on-Pt}(111)\}} - \text{En}_{\{\text{Pt}(111)\}} - \text{En}_{\{\text{CD-on-Pt}(100)\}} + \\ \text{En}_{\{\text{Pt}(100)\}} = \text{En}_{(\text{ADS})}$$

where $\text{En}_{\{\text{CD-on-Pt}(111)\}}$ was the calculated energy of the system composed by CD adsorbed on Pt(111), $\text{En}_{\{\text{CD-on-Pt}(100)\}}$ was the calculated energy of the system composed by CD adsorbed on Pt(100), $\text{En}_{\{\text{Pt}(111)\}}$ and $\text{En}_{\{\text{Pt}(100)\}}$ were the calculated energies of the Pt(111) and Pt(100) surfaces, and finally $\Delta \text{En}_{(\text{ADS})}$ was the calculated difference between the adsorption of CD on Pt(111) and

Pt(100) surface. Note that the energy of CD is not present since it cancels in the summation. The Surface Open(4) conformation of adsorbed CD was chosen since it resulted in the most likely geometry for the formation of surface docking structures, as shown elsewhere.[13]

3. Results and Discussion

3.1. Characterization of Model Catalysts. Variation of the Pt:PAA ratio in the colloid synthesis leads to different particle shape distributions, as illustrated by the TEM pictures in Figure 2. The average diameter of 10 nm is very similar for all samples, but the preferred shape varies from mainly cubic and truncated cubic particles in Pt-1 over mainly cubooctahedral (Pt-2) to truncated octahedral and octahedral particles (Pt-3), in good agreement with literature data.[46,54,70] It has been shown by HRTEM,[54] CO adsorption microcalorimetry[46] and electrochemical methods[46] for Pt colloids prepared by this method that the presence of cubic particles is related to a high fraction of Pt{100} faces, whereas hexagonal particles such as tetrahedrons and octahedrons expose preferentially Pt{111} terraces.

The average particle size and the shape distribution are well maintained during deposition of the colloids onto silica (Table

(63) Liu, D.; Nocedal, J. *Siam. J. Sci. Stat. Comp.* **1989**, *10*, 1–17.
(64) Nocedal, J. *Math. Comput.* **1980**, *35*, 773–782.
(65) Shanno, D.; Kettler, P. *Math. Comput.* **1970**, *24*, 657–664.
(66) Goldfarb, D. *Math. Comput.* **1970**, *24*, 23–26.
(67) Broyden, C. *Math. Comput.* **1970**, *24*, 365–382.
(68) Santarossa, G.; Iannuzzi, M.; Vargas, A.; Baiker, A. *Chem. Phys. Chem.* **2008**, *9*, 401–413.
(69) Vargas, A.; Baiker, A. *J. Catal.* **2007**, *247*, 387.

(70) Inaba, M.; Ando, M.; Hatanaka, A.; Nomoto, A.; Matsuzawa, K.; Tasaka, A.; Kinumoto, T.; Iriyama, Y.; Ogumi, Z. *Electrochim. Acta* **2006**, *52*, 1632–1638.

Table 1. Characteristics of the Supported Pt Nanoparticles and the Reference Catalyst Pt/Al$_2$O$_3$

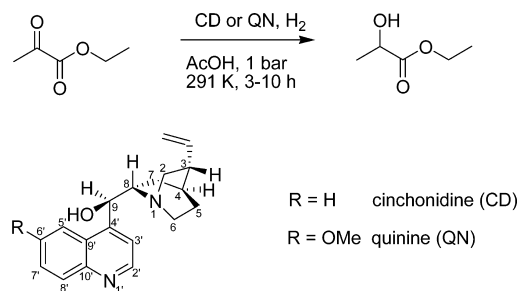| sample	Pt, wt %	d_{av}, nm	dominant shape	Pt{111}/ Pt{100}	metal dispersion[a]
Pt-1/SiO$_2$	4.6 ± 0.5	9.9 ± 1.2	cubic	0.23	0.13
Pt-1/Al$_2$O$_3$	4.5 ± 0.6	n.d.[b]	n.d.[b]	n.d.[b]	n.d.[b]
Pt-2/SiO$_2$	4.5 ± 0.4	9.8 ± 1.0	cubooctahedral	1.05	0.13
Pt-3/SiO$_2$	4.7 ± 0.5	10.2 ± 1.0	octahedral	2.44	0.14
Pt/Al$_2$O$_3$ (reference)	5.8 ± 0.3	3.2 ± 1.2	spherical	n.d.[b]	0.32

[a] Atomic ratio of surface Pt atoms to the total number of Pt atoms. [b] Not determined.

1). A detailed evaluation based on analyzing approximately 600 to 1000 particles for each sample[35,71] can be found in the Supporting Information. The most important characteristic is the {111}/{100} ratio of exposed Pt crystal faces as estimated by TEM; it increases from Pt-1/SiO$_2$ over Pt-2/SiO$_2$ to Pt-3/SiO$_2$ (see Table 1). Note that not only the fraction of terrace sites such as Pt{111} and Pt{100} changes, but also the amount and type of low coordinated sites (e.g., edge and corner sites, see Supporting Information) are slightly different. Their proportion to the total number of surface atoms is, however, rather small due to the high average particle diameter. The average particle size of the reference Pt/Al$_2$O$_3$ is considerably smaller, and the particle shape is nearly spherical. Thus, both Pt{100} and Pt{111} terraces are present, but due to the lower particle size, the amount of low coordinated sites is significantly higher compared to the self-prepared catalysts.[29]

Characterization of the supported catalysts by XPS revealed the absence of any impurity except a significant amount of organic residue, which is attributed to the colloid stabilizer PAA adsorbed strongly on the catalyst surface. The amount of carbon was identical in all self-prepared samples. The peak positions for Si 2p (103.4 eV), O 1s (532.6−532.8 eV), Pt 4$f_{7/2}$ (70.5−70.7 eV), and C 1s (284.7−285 eV) are in agreement with literature data for SiO$_2$, Pt^0, and poly(acrylic acid) (PAA).[72]

The presence of residual PAA molecules on the Pt surface was further elucidated by DRIFT spectroscopy of CO adsorption. The spectra obtained after CO adsorption and removal of gas phase CO by purging with Ar were compared to the corresponding spectrum obtained on the reference Pt/Al$_2$O$_3$. The exceptionally low intensity of the signal related to atop adsorption of CO on Pt in the case of all self-prepared samples indicates that the Pt surface is efficiently blocked by the colloidal stabilizer, in agreement with recent reports on the strong adsorption of the colloid stabilizer.[52,73−75] This interpretation is underlined by the unusually low frequency of this CO signal (2064−2065 cm^{-1}) corresponding to the formation of isolated CO islands typical for extremely low surface coverage.[76] Note that removal of PAA is possible by oxidative and reductive catalyst pretreatments at elevated temperature, but no such treatment was necessary before asymmetric hydrogenation of

(71) VanHardeveld, R.; VanMontfoort, A. *Surf. Sci.* **1966**, *4*, 396–430.
(72) Wagner, C. D.; Naumkin, A. V.; Kraut-Vass, A.; Allison, J. W.; Powell, C. J.; Rumble, J. J. R. NIST X-ray Photoelectron Spectroscopy Database (http://srdata.nist.gov/xps/).
(73) Bratlie, K. M.; Lee, H.; Komvopoulos, K.; Yang, P.; Somorjai, G. A. *Nano Lett.* **2007**, *7*, 3097–3101.
(74) Liu, D.; Gao, J.; Murphy, C. J.; Williams, C. T. *J. Phys. Chem. B* **2004**, *108*, 12911–12916.
(75) Crump, C. J.; Gilbertson, J. D.; Chandler, B. D. *Top. Catal.* **2008**, *49*, 233–240.
(76) Krebs, H.-J.; Lüth, H. *Appl. Phys.* **1977**, *14*, 337–342.

Scheme 1. Hydrogenation of Ethyl Pyruvate in the Presence of Cinchona Alkaloids

Table 2. Hydrogenation of Ethyl Pyruvate: Initial Rates (TOFs) and Enantiomeric Excesses (ee's) to (*R*)-Lactate at Full Conversion

catalyst	chiral modifier	ee, %	TOF, h^{-1}	rate enhancement
Pt/Al$_2$O$_3$ (reference)	−	−	156	−
	CD	80	1200	7.7
	QN	85	1480	9.5
Pt-1/SiO$_2$ {100}	−	−	126	−
	CD	72	530	4.2
	QN	77	850	6.7
Pt-1/Al$_2$O$_3$ {100}	−	−	143	−
	CD	71	570	4.0
	QN	76	840	5.9
Pt-2/SiO$_2$ {100}+{111}	−	−	147	−
	CD	78	730	5.0
	QN	83	1380	9.4
Pt-3/SiO$_2$ {111}	−	−	127	−
	CD	86	1350	10.6
	QN	92	1890	14.8

ketones, as no significant poisoning effect under reaction conditions, in the liquid phase, was observed (see the next section).

3.2. Enantioselective Hydrogenation of Activated Ketones. The performance of the supported Pt nanoparticles was investigated in the enantioselective hydrogenation of activated ketones. The results related to the hydrogenation of ethyl pyruvate (Scheme 1) are collected in Table 2.

This reaction is known to be disturbed by side reactions when inappropriate conditions are chosen.[77] Aldol condensation catalyzed by the Pt surface, the amine modifier, and the basic sites on the alumina support leads to high molecular weight byproducts that partially block the active sites and distort the results. To suppress the side reactions it is important to use acetic acid as solvent, maintain a high surface hydrogen concentration during reaction (i.e., to avoid hydrogen "starvation" conditions), and add the pyruvate directly before starting the reaction.

In Table 2 the reaction rates are characterized by the TOFs, related to the total number of surface Pt atoms. The observed TOFs for the unmodified reaction leading to racemic products are very similar on all four self-prepared catalysts, despite their different Pt particle shapes. All values fall in a relatively narrow range of 136.5 ± 10.5 h^{-1}, where the deviations do not exceed the expected standard deviation of determining the specific reaction rate (±5−10%). Clearly, pyruvate hydrogenation on Pt is a structure insensitive reaction.

Importantly, no significant difference in reaction rates was observed by replacing the silica support with alumina (compare

(77) von Arx, M.; Mallat, T.; Baiker, A. *Top. Catal.* **2002**, *19*, 75–87.

Pt-1/SiO$_2$ and Pt-1/Al$_2$O$_3$). In addition, the ee's are also very similar; the deviations do not exceed the estimated error of the analysis (±0.5%). This is an indication that the support effect is minor and the self-prepared silica-supported catalysts can be compared to the widely used reference catalyst Pt/Al$_2$O$_3$.

In the absence of a chiral modifier, the reference catalyst Pt/Al$_2$O$_3$ is only slightly more active than the self-prepared catalysts. The small difference indicates that the residual colloid stabilizer that diminished the adsorption of CO on Pt at the solid/gas interface has only a minor poisoning effect at the solid/liquid interface during pyruvate hydrogenation. This astonishing observation may be explained by the efficient competition at the solid/liquid interface between the colloid stabilizer and the reaction components: the solvent,[74] the substrate, and hydrogen. In particular, the effect of acetic acid solvent seems to be important due to its chemical similarity to the polycarboxylic acid type stabilizer. Thus, investigation of the enantioselective hydrogenation of ethyl pyruvate on the as-prepared catalysts is possible without any forceful pretreatment, which could result in particle agglomeration and restructuring of the Pt surface.

Addition of the chiral modifier induced a considerable rate enhancement ("ligand acceleration")[78] compared to the unmodified reaction (Table 2). The rate enhancement varies in the range 4−15 and strongly depends on the crystallographic face exposed on Pt and also on the modifier structure. The rate acceleration correlates well with the Pt particle shape: it increases with the increasing Pt{111}/Pt{100} ratio on the self-prepared catalysts. The Pt/Al$_2$O$_3$ reference catalyst is characterized by medium rate enhancement. This catalyst exposes both Pt{100} and Pt{111} faces similar to Pt-2/SiO$_2$ but contains a higher fraction of low coordinated Pt surface atoms. This comparison suggests that the relative amount of low coordinated Pt sites has a negligible effect on the catalyst performance; however, a reliable prediction of the possible structure sensitive behavior of the asymmetric hydrogenation on very small Pt clusters is impossible. The observed rate enhancement in the presence of CD is in good agreement with literature values.[79]

The rate enhancement and enantioselectivity, both induced by addition of the chiral modifier, are clearly correlated; i.e., catalysts with a higher Pt{111}/Pt{100} ratio are more reactive and afford higher ee's. In the best case scenario, over 90% ee was achieved on Pt-3/SiO$_2$ which catalyst exposes the highest relative amount of Pt{111} and shows the strongest rate acceleration. Note that a positive correlation between the reaction rate and enantioselectivity has frequently been observed for supported Pt catalysts, and it is attributed to the common mechanistic origin of the two phenomena.[1,80,81]

In Table 2 the ee's determined at full conversion are given. Variation of the enantioselectivity with time (and conversion) is illustrated in Figure 3 using Pt/Al$_2$O$_3$ and Pt-2/SiO$_2$ catalysts. These two catalysts behaved similarly in many respects, but there is a remarkable difference in the initial transient period until ∼20−30% conversion. In case of the reference catalyst Pt/Al$_2$O$_3$ variation of the ee with conversion is small, while there is a rapid selectivity enhancement in the early stage of the reaction over the silica-supported Pt nanoparticles. Above 30%
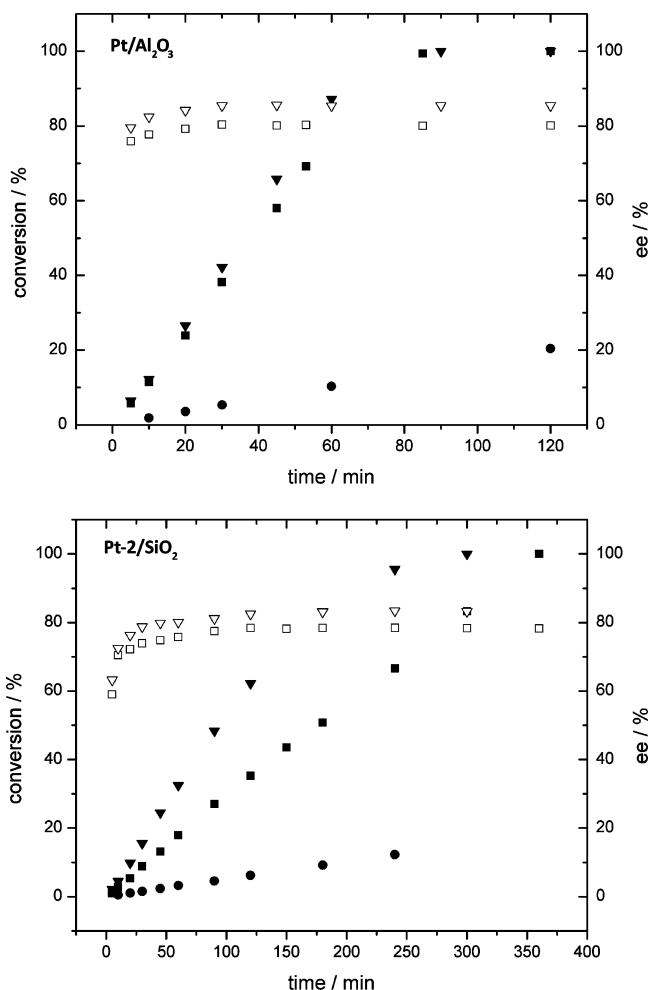
(78) Garland, M.; Blaser, H. U. *J. Am. Chem. Soc.* **1990**, *112*, 7048.
(79) Blaser, H. U.; Jalett, H. P.; Monti, D. M.; Reber, J. F.; Wehrli, J. T. *Stud. Surf. Sci. Catal.* **1988**, *41*, 153.
(80) Blaser, H. U.; Jalett, H. P.; Müller, M.; Studer, M. *Catal. Today* **1997**, *37*, 441–463.
(81) Szöllösi, G.; Cserényi, S.; Fülöp, F.; Bartók, M. *J. Catal.* **2008**, *260*, 245–253.

Figure 3. Time dependence of conversion (filled symbols) and ee (empty symbols) in the hydrogenation of ethyl pyruvate on Pt/Al$_2$O$_3$ reference catalyst (top) and Pt-2/SiO$_2$ (bottom). Symbols: circles for the unmodified reaction, squares in the presence of CD, and triangles in the presence of QN.

conversion the enantioselectivity remains practically constant for both catalysts. The behavior of Pt-1/SiO$_2$ and Pt-3/SiO$_2$ was very similar to that of Pt-2/SiO$_2$ (see Supporting Information). The changes in the enantioselectivity in the early stage of the hydrogenation of pyruvate esters and other activated ketones are commonly related to changes in the surface composition of the reactants and to the removal of some impurities.[1,2] The significantly stronger initial transient period in reactions over the silica-supported Pt nanoparticles compared to that on the reference Pt/Al$_2$O$_3$ indicates that partial removal of the polymeric stabilizer from the surface of Pt nanoparticles plays an important role. It is expected that the presence of strongly adsorbed foreign species disturbs the modified reaction more than that of the unmodified (racemic) hydrogenation, since the former requires a much bigger ensemble of Pt surface sites. Thus, (partial) removal of the stabilizer by the competing adsorption of hydrogen, substrate, modifier, and solvent should lead to enhanced enantioselectivity.
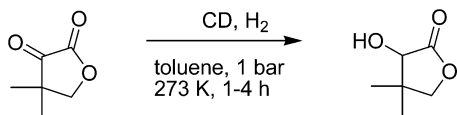
The second test reaction was the hydrogenation of ketopantolactone in the presence of CD (Table 3). An advantage of this substrate is the absence of an H atom in α-position to the keto-carbonyl group, the structural difference of which reduces the number of possible side reactions (aldol condensation), compared to the hydrogenation of ethyl pyruvate. Moreover,

Table 3. Hydrogenation of Ketopantolactone: Initial Rates (TOFs) and Enantiomeric Excesses (ee's) at Full Conversion

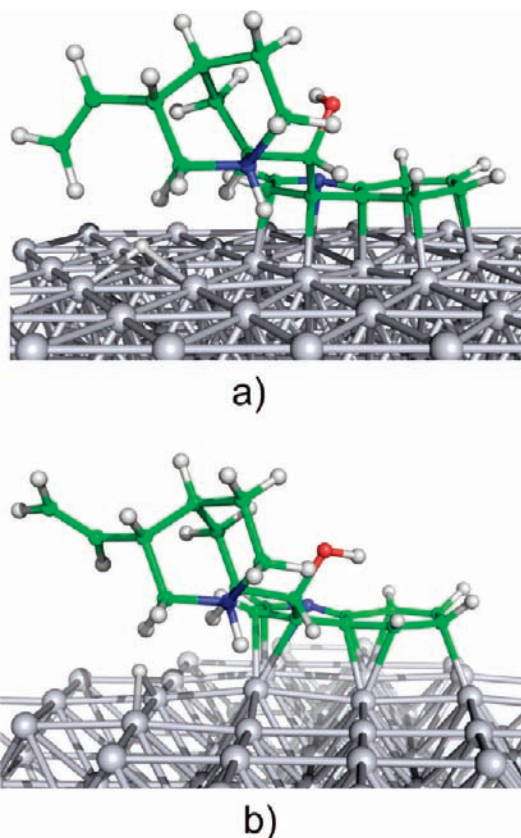| catalyst	chiral modifier	TOF, h^{-1}	rate enhancement	ee, %	ee,[a] %
Pt/Al$_2$O$_3$	−	250	−	−	−
(reference)	CD	500	2.0	45	76
Pt-1/SiO$_2$	−	140	−	−	−
{100}	CD	445	3.2	47	72
Pt-2/SiO$_2$	−	145	−	−	−
{100}+{111}	CD	610	4.2	53	78
Pt-3/SiO$_2$	−	125	−	−	−
{111}	CD	630	5.0	61	81

[a] Measured at 70 bar and 264 K.

ketopantolactone shows no significant tendency to decarbonylation on Pt.[82]

Despite of the considerably different reaction conditions, the positive correlation between the increasing {111}/{100} ratio of exposed Pt crystal faces and the reaction characteristics (rate enhancement and enantioselectivity) is valid also in this reaction. The rate of the unmodified reaction on all three homemade catalysts is very similar, the deviation does not exceed the expected error (TOF = 135 ± 10 h^{-1}). Hence, also in this case the hydrogenation of the C=O bond on the unmodified Pt surface is structure insensitive, and addition of CD induces significant, structure-specific rate acceleration and enantioselectivity. Overall, the observed ee's are somewhat lower than the best values reported for both substrates,[55,56] because the beneficial catalyst prereduction under elevated temperature could not be used here to avoid changes in the Pt nanoparticle shape. Note that the performance of Pt-3/SiO$_2$ containing the highest Pt{111}/Pt{100} ratio is superior to the as-received reference Pt/Al$_2$O$_3$ under both conditions applied.

3.3. Adsorption of Cinchonidine on Pt(111) and Pt(100) Surfaces. It has been shown elsewhere[13,69,83] that due to its conformational complexity CD can have several adsorption modes on a platinum surface. Both experimental and theoretical evidences support the view that the Surface OPEN(4) (SO(4)) conformation is the most populated (in terms of fractional coverage) after adsorption.[13] In the present study we are mainly interested in the difference between the adsorption energy of CD on Pt(111) and Pt(100) surfaces. Figure 4 shows CD adsorbed SO(4) on Pt(111) and Pt(100) (Cartesian coordinates of both adsorbed structures are available as Supporting Information). At the level of theory used, CD is more strongly adsorbed on Pt(100) than on Pt(111) by ca. 155 kJ/mol. This is reflected by the larger amount of charge transfer from the metal to the adsorbed molecule.[68] Lowdin charge analysis[84] shows in fact that back-donation from Pt(100) to the adsorbate is larger than that from Pt(111) by ca. 0.2 e.

In relation to structural parameters, it has already been shown that upon adsorption of CD the quinoline moiety becomes

(82) Bonalumi, N.; Bürgi, T.; Baiker, A. *J. Am. Chem. Soc.* **2003**, *125*, 13342–13343.
(83) Vargas, A.; Baiker, A. *J. Catal.* **2006**, *239*, 220–226.
(84) Lowdin, P.-O. *J. Chem. Phys.* **1950**, *18*, 365–375.

Figure 4. CD adsorbed on Pt(111) (a) and on Pt(100) (b).

Table 4. Bond Lengths (in Å) of the Quinoline Moiety (Anchoring Group) in the Adsorbed CD on Pt(111) and Pt(100) Surfaces (Figure 4a and b, Respectively)[a]

	N(1')C(2')	C(2')C(3')	C(3')C(4')	C(4')C(9')	C(9')C(10')	C(9')C(5')
Pt(111)	1.371	1.431	1.487	1.505	1.476	1.491
Pt(100)	1.374	1.468	1.441	1.489	1.487	1.460

	C(5')C(6')	C(6')C(7')	C(7')C(8')	C(8')C(10')	C(10')N(1')	average
Pt(111)	1.471	1.432	1.468	1.485	1.403	1.456
Pt(100)	1.472	1.490	1.467	1.459	1.459	1.454

[a] Atom numbering refers to Scheme 1.

Table 5. Bond Distances (in Å) between the Atoms of the Adsorbed Quinoline (Anchoring Group) and Pt Atoms, for CD Adsorption on Pt(111) and Pt(100) Surfaces (Figure 4a and b, Respectively)[a]

	N(1')Pt	C(2')Pt	C(3')Pt	C(4')Pt	C(9')Pt	C(5')Pt
Pt(111)	2.231	2.332	2.184	2.174	2.191	2.163
Pt(100)	2.397	2.161	2.157	2.234	2.159	2.176

	C(6')Pt	C(7')Pt	C(8')Pt	C(10')Pt	average
Pt(111)	2.214	2.212	2.159	2.205	2.207
Pt(100)	2.147	2.157	2.165	2.193	2.195

[a] Atom numbering refers to Scheme 1.

remarkably distorted.[14] In particular, bonds are elongated and the planarity of the aromatic system is lost (rehybridization). Structural parameters that characterize the chemisorptions of CD on Pt have been summarized in Tables 4–6. Table 4 gives a list of the bond lengths of quinoline (anchoring group) upon adsorption on Pt(111) and Pt(100). Table 6 gives a list of the deviation from planarity of the C–H and C–C bonds of

Table 6. Rehybridization of C–H and C–C Bonds of Quinoline for CD Adsorption on Pt(111) and Pt(100) Surfaces (Figure 4a and b, Respectively)[a]

	C(2′)H	C(3′)H	C(4′)C(9)	C(5′)H	C(6′)H	C(7′)H
Pt(111)	11	23.8	47	42.9	18.9	18.3
Pt(100)	29.9	26.8	21.9	16.2	41.1	41.0

	C(8′)H	average
Pt(111)	43.8	29.4
Pt(100)	21.2	28.3

[a] Atom numbering refers to Scheme 1. The values (degrees) indicate the deviation of dihedral angles from planarity.

quinoline (rehybridization). Note that the stronger adsorption of CD on Pt(100) is reflected by the smaller average distance between the atoms of the anchoring group and the Pt atoms of the surface. In fact, this results in 2.21 Å for CD on Pt(111) and 2.19 Å for CD on Pt(100) (Table 5). Other average parameters, namely internal bond lengths (Table 4) and rehybridization (Table 6), do not change significantly.

A closer examination of Tables 4–6 reveals that major changes occur at the level of the C(6′) and C(7′) carbon atoms, on the homoaromatic ring of quinoline, when passing from adsorption on Pt(111) to adsorption on Pt(100). This site of the molecule upon adsorption on Pt(100) is closer to the metal, strongly rehybridized, and the bond length C(6′)–C(7′) is remarkably elongated. This is due to the adsorption topology, itself conditioned by the surface topology, and indicates that the homoaromatic ring of quinoline undergoes the most remarkable structural changes on the strongest adsorption site.

3.4. Hydrogenation of Cinchonidine Studied by UV Spectroscopy. Adsorption of cinchona alkaloids on the metal surface via the quinoline ring, the so-called "anchoring moiety", is a key element of all mechanistic models developed for ketone hydrogenation on Pt.[1] The enantioselectivity is affected by both the strength and the mode of adsorption: flat (π-bonded) or tilted (N-lone pair bound). The former adsorption mode is assumed to be more favorable to achieve high ee's. An indirect way to characterize the adsorption strength of the alkaloid under reaction conditions is to investigate the rate of saturation of the quinoline ring.[85] Note that the vinyl group of the alkaloid in the 10–11 position is hydrogenated much faster, but this function is not involved in the enantioselection and this reaction will not be discussed here.

Hydrogenation of CD on all three silica-supported Pt colloids was followed with UV spectroscopy. The reaction conditions were identical to those of pyruvate hydrogenation at ambient pressure, except for the absence of the substrate. The rate of saturation of the aromatic ring of CD is illustrated in Figure 5 for Pt-1/SiO$_2$ and Pt-3/SiO$_2$, which possess the lowest and highest ratio of Pt{111}/Pt{100} exposed faces, respectively. (The corresponding UV spectra of the hydrogenation of CD over Pt-1/SiO$_2$ and Pt-3/SiO$_2$ are shown in the Supporting Information.) The sharp signal at 315 nm and the broader feature at ∼305 nm are specific for the extended aromatic system of quinoline.[86] The decreasing intensity of the signal at 315 nm with time is attributed to the conversion of the aromatic ring of CD. This reaction is efficiently catalyzed by Pt-1/SiO$_2$ (Figure 5, left side); almost no CD is left after 5 h. Pt-2/SiO$_2$ and Pt/

Al$_2$O$_3$ were less active (see support information), and the quinoline ring was barely converted on Pt-3/SiO$_2$ (Figure 5, right). After 5 h the concentration of CD in solution was higher than that in the hydrogenation on Pt-1/SiO$_2$ after only 30 min.

The main hydrogenation product observed in the presence of acetic acid is 5′,6′,7′,8′,10,11-hexahydrocinchonidine via hydrogenation of the homoaromatic ring of the quinoline moiety and the vinyl group.[85,86] This species gives a UV signal at ∼270 nm as can be seen in Figure 4 for Pt-1/SiO$_2$. Significant amounts of 1′,2′,3′,4′,10,11-hexahydrocinchonidine (broad feature at 295 nm),[86] formed via hydrogenation of the heteroaromatic ring of quinoline, and that of the fully saturated CD cannot be excluded by these experiments. On Pt-3/SiO$_2$ no corresponding signal of a partially hydrogenated quinoline moiety was observed, in good agreement with the persistency of the CD signal.

The study reveals an unprecedented high stability toward hydrogenation of the quinoline anchoring moiety of the alkaloid on the Pt{111} face. The reactivity toward aromatic hydrogenation increases with the increasing Pt{100}/Pt{111} ratio of exposed crystal faces.

For comparison, structure sensitivity in the hydrogenation of benzene on supported Pt nanoparticles of different shapes has recently been reported.[73] While on catalysts containing almost exclusively Pt particles of cubic shape, i.e., on Pt{100}, the fully hydrogenated cyclohexane was the only product, in the presence of Pt{111} and Pt{100} (on samples containing cubooctahedral particles) both cyclohexene and cyclohexane were observed. Unfortunately, no data on the hydrogenation of quinoline and its derivatives are available yet.

It should be emphasized that the theoretical calculations discussed previously (Tables 4–6) show that upon adsorption on a Pt(100) surface the homoaromatic ring of the quinoline moiety undergoes a remarkably larger distortion and deviation from aromaticity as compared to the same adsorption on Pt(111). The C(6′)–C(7′) bond of the anchoring moiety is especially elongated and rehybridized on Pt(100), and from a theoretical point of view it should be especially sensitive to saturation. This expectation has been confirmed with the above-noted faster saturation of the homoaromatic moiety of the quinoline fragment of CD on the Pt{100} rich catalyst. The correlation between the adsorption strength of aromatics and the hydrogenation rate on Pt can probably be attributed to the weakening of the aromaticity, and therefore of the aromatic stability, that is directly proportional to the strength of the interaction of the hydrocarbon to the metal.

Note that hydrogenation of the cinchona alkaloid modifier has only minor importance in practical catalysis, since saturation of the aromatic ring of the alkaloid weakens the adsorption on Pt, the converted molecule desorbs from the surface, and another CD molecule replaces it.[1,2] Hence, the slower the target reaction relative to the transformation of CD, the higher excess of the alkaloid is necessary to modify the Pt surface and avoid any significant change in the enantiomeric excess with time (or conversion). The plots in Figure 3 demonstrate that the experimental conditions (the concentration of the alkaloid modifier) were properly chosen, since the ee did not drop at high conversion, which would be an indication of an insufficient coverage of Pt by the modifier.

3.5. Origin of Structure Sensitivity. In the unmodified hydrogenation of ethyl pyruvate (Table 2) similar TOFs in the range 126–156 h^{-1} were observed on all four self-prepared catalysts possessing the same Pt particle size (ca. 10 nm) and dominantly cubic, cubooctahedral, or octahedral shapes, and on

(85) Huck, W.-R.; Bürgi, T.; Mallat, T.; Baiker, A. *J. Catal.* **2003**, *216*, 276–287.
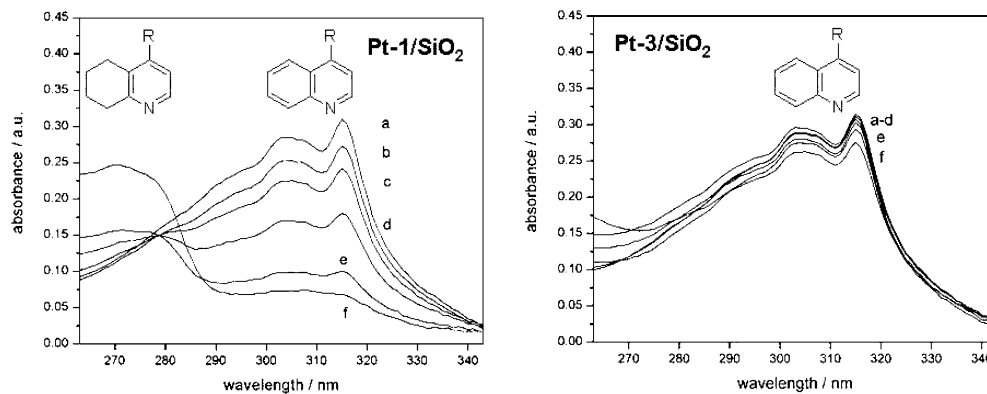(86) Hoxha, F.; Mallat, T.; Baiker, A. *J. Catal.* **2007**, *248*, 11–19.

Figure 5. Hydrogenation of the aromatic ring of CD followed by UV spectroscopy on Pt-1/SiO$_2$ and Pt-3/SiO$_2$. Curve (a) is obtained after adsorption on the catalyst for 5 min under nitrogen; hydrogenation for 30 (b), 60 (c), 120 (d), 210 (e), and 300 min (f).

a commercial reference catalyst with smaller spherical Pt particles (3.2 nm). Evidently, hydrogenation of the keto-carbonyl group of ethyl pyruvate is structure insensitive: the reaction rate depends neither on the preferred Pt particle shape nor on the average particle size in the investigated range.

Introduction of the chiral modifiers CD and QN turned the reaction to structure sensitive, and on all samples remarkably higher rates, by a factor of 4−15, were achieved compared to the unmodified reaction. Additionally, there is an unambiguous positive correlation between the Pt{111}/Pt{100} ratio of exposed crystal faces (Pt-3/SiO$_2$ > Pt-2/SiO$_2$ ≈ Pt/Al$_2$O$_3$ > Pt-1/SiO$_2$) and the rate and enantioselectivity of the reaction. In contrast, the fraction of Pt defect sites (coordination number below 8) seems to be unimportant.

Recently, there has been some debate in the literature on the origin of rate enhancement and its possible correlation with the enantioselection.[87,88] Note that our observation of a clear correlation between the rate acceleration and the enantioselectivity seems to be in agreement with recent catalytic and surface science studies.[81,89]

The role of steps and {100} terrace sites on Pt in pyruvate hydrogenation was previously investigated by the preferential deposition of Bi and S adatoms onto the metal surface of Pt/graphite.[90] Based on the combined electrochemical and catalytic study, it was proposed that the enantioselection would be more efficient in the vicinity of step sites than those located on terraces. It is questionable, however, whether the specific adsorption of single Bi or S atoms is a reliable model for the adsorption of the bulky CD−pyruvate ester complex, the formation of which is necessary to induce enantioselection.[1−4,17] As estimated from theoretical calculations, an active site ensemble of approximately 20−25 Pt atoms is necessary to accommodate the interacting complex.[9] In addition, a serious catalyst deactivation and poor enantioselectivities were observed under high pressure conditions that were probably due to hydrogenolysis of the solvent dichloromethane.[91] Hydrochloric acid catalyzes the hydrolysis of pyruvate esters, and it is a good catalyst for the dimerization and oligomerization of activated ketones. Blocking of a dominant fraction of Pt surface sites by

the resulting high molecular weight byproducts may have a larger influence on the enantioselection than that of the Bi or S adatoms.

The observed trend of the higher rate and enantioselectivity on catalysts exposing higher Pt{111}/Pt{100} ratios is confirmed in the hydrogenation of another activated ketone, ketopantolactone, under different conditions (Table 3). In ketopantolactone, there is no H atom in α-position to the keto group and no significant side reactions could be detected by ATR-IR spectroscopy.[82] This difference supports our interpretation that the structure sensitivity is an intrinsic feature of the enantioselective hydrogenation of α-ketoesters and lactones on Pt and not the result of undetected side reactions.[88]

In the presence of CD and QN, the structure insensitive hydrogenation of ketones becomes structure sensitive. Further investigation revealed that hydrogenation of the aromatic ring of the chiral modifier is also structure sensitive (Figure 5). Under the conditions applied, almost no transformation of the homoaromatic ring of the quinoline fragment of CD was observed on the catalyst containing the highest Pt{111}/Pt{100} ratio (Pt-3/SiO$_2$) and the rate increased with the increase in the fraction of the Pt{100} face exposed.

DFT calculations showed that the probable origin of structure sensitivity is the different adsorption strength, and the consequent major distortion from aromaticity (and therefore bond weakening), of the alkaloid on the Pt(100) with respect to the Pt(111) surfaces (Figure 4, Tables 4−6). The major consequence of this different adsorption is an especially pronounced elongation of the C(6′)−C(7′) bond, as well as strong rehybridization at this site of the molecule (homoaromatic moiety of the quinoline).

Hydrogenation experiments show that exactly this part of the molecule is sensitive to saturation on Pt(100) rich catalysts. Although enantioselectivity is a more complex process than the adsorption behavior of the chiral modifier, it has been previously shown that saturation of the anchoring moiety of a chiral modifier leads to desorption of the modifier and to lower enantioselectivity.[92] In other words, an efficient chiral modification requires the formation of chiral sites which are stable under hydrogenation conditions, and Pt{100} rich catalysts are revealed to be less apt to stably accommodate modifiers based on quinoline as anchoring unit. That is, the stronger interaction

(87) Toukoniitty, E.; Murzin, D. Y. *J. Catal.* **2007**, *251*, 244–245.
(88) Mallat, T.; Baiker, A. *J. Catal.* **2007**, *251*, 246–248.
(89) Lavoie, S.; Lalibert, M.-A.; Mahieu, G.; Demers-Carpentier, V.; McBreen, P. *J. Am. Chem. Soc.* **2007**, *129*, 11668–11669.
(90) Jenkins, D. J.; Alabdulrahman, A. M. S.; Attard, G. A.; Griffin, K. G.; Johnston, P.; Wells, P. B. *J. Catal.* **2005**, *234*, 230–239.
(91) Meier, D. M.; Ferri, D.; Mallat, T.; Baiker, A. *J. Catal.* **2007**, *248*, 68–76.

(92) Baiker, A.; Blaser, H. U. In *Handbook of Heterogeneous Catalysis*; Ertl, G., Knözinger, H., Weitkamp, J., Eds.; Wiley-VCH: Weinheim, Germany, 1997; Vol. 5, p 2422.

of the quinoline moiety of CD with the Pt(100) face compared to Pt(111) reduces its stability against hydrogenation and promotes fast deterioration of chirally active sites.

4. Summary

The present study reveals for the first time that enantioselective hydrogenation on chirally modified Pt nanoparticles is shape selective: both the reaction rate and the enantioselectivity increase with the increase in the Pt{111} to Pt{100} ratio. The origin of structure sensitivity is traced to the different adsorption behavior of the alkaloid modifier on these crystallographic faces, which in turn affects the interaction with the substrate in the activated complex during hydrogen uptake. In addition, the present work provides unambiguous experimental evidence for the phenomenon of "ligand acceleration" in heterogeneous catalysis and its dependence on the crystallographic face of Pt.

It has to be emphasized that due to the individual particle shape distributions not exclusively Pt{100} and Pt{111} faces are exposed in Pt-1/SiO$_2$ and Pt-3/SiO$_2$, respectively. Each sample contains terraces of both types and additional low coordination sites. Therefore, the differences between the theoretical enantio-differentiating ability of ideal Pt(100) and Pt(111) single crystal surfaces are expected to be considerably bigger than those observed here with supported Pt nanoparticles.

The results provide a scientific basis for the design of highly enantioselective, active, and stable enantioselective catalysts.

Supporting Information Available: Particle size and shape distributions of samples Pt-1/SiO$_2$, Pt-2/SiO$_2$, and Pt-3/SiO$_2$; conversion vs time plots (including ee) of the ambient pressure hydrogenation of ethyl pyruvate; Cartesian coordinates of optimized geometry of CD on Pt surfaces; UV spectra of CD hydrogenation on Pt/Al$_2$O$_3$ and Pt-2/SiO$_2$; DRIFT spectra of CO adsorption on the catalysts. This material is available free of charge via the Internet at http://pubs.acs.org.

JA9043328